Markov state modeling reveals competing collective hydrogen bond rearrangements in liquid water

R. Schulz,[1] Y. von Hansen,[1] J. O. Daldrop,[1] J. Kappler,[1] F. Noé,[2] and R. R. Netz[1]

[1] *Department of Physics, Freie Universität Berlin, 14195 Berlin, Germany*
[2] *Department of Mathematics and Computer Science, Freie Universität Berlin, 14195 Berlin, Germany*

(Dated: February 22, 2018)

We construct a Markov state model for the dynamic rearrangement of the local hydrogen bond network in liquid water. The model is based on trajectories from classical molecular dynamics simulations and accounts for the dynamics of relative angular and separation coordinates of water molecules. We analyze first the conformational subspace of three water molecules and find five well separated dynamic modes with reaction times in the 2 - 5 ps range, which correspond to different interchanges of hydrogen bond donor and acceptors, followed by an entire continuum spectrum of modes. We then analyze the switching of one hydrogen bond between two water molecules and derive the complete transition network. The most probable pathway corresponds to a direct switch without an intermediate, in agreement with previous studies. However, a considerable fraction of paths proceeds along different intermediate states that involve alternative hydrogen bonds or unbound states.

I. INTRODUCTION

Water plays a key role for many processes governing biological, chemical, and physical processes [1]. On the microscopic level the water dynamics involves the forming and breaking of hydrogen bonds (H-bonds) which is important for understanding protein [2] and membrane dynamics [3]. The current understanding of H-bond dynamics seems inferior compared to hydrophobic solvation [4–6]. Even the mechanism of breaking and forming a single H-bond between two water molecules that are embedded in liquid water still poses open questions.

Based on transition path sampling, it was suggested that in half of the H-bond breaking events a new H-bond is formed right after [7], partly confirming Stillinger's switching-of-allegiance scenario of the local hydrogen bonding dynamics [8]. According to the classical view, the reorientation of a water molecule is described by a diffusion model originally introduced by Debye [9]. In this model, water reorientation is diffusive and driven by angular Brownian motion, so when an H-bond is broken it performs an angular overdamped motion until it finds a new partner. However, in [10–13] it has been shown based on molecular dynamics simulations that the reorientation of an H-bond donor occurs typically through an abrupt angular jump, which is supported experimentally by neutron scattering [14, 15] and 2D-IR spectroscopy [12, 16, 17]. The prevalence of abrupt rotations seems to suggest that non H-bonded configurations, also referred to as dangling H-bonds, are inherently unstable and should only appear as short-lived transient states that either rebond with its initial H-bond partner or quickly engage in a new H-bond with a different partner [18]. Insight into H-bond dynamics has also been obtained from nuclear quantum simulations [19–22], where concerted rotations of water molecules in isolated water clusters have been observed and H-bond cooperativity has been identified as an important element. H-bond network rearrangements have also been studied by femtosecond IR spectroscopy and characterized by time scales ranging in the sub-picosecond to picosecond range [23–26] or in the 5 to 15 ps range [27].

What is missing is a method to unambiguously classify local H-bond kinetics based on simulation trajectories in an unbiased fashion. The reason for this lack is the overwhelming state space, since the relative conformation of only two water molecules is described by a six-dimensional space (one separation coordinate, two relative angular coordinates and 3 relative orientational coordinates). Consequently, the state space of three water molecules, the minimal system where collective H-bond switching can be studied, is 12-dimensional, which makes the direct observation of H-bond dynamics in simulation trajectories prohibitively difficult. We demonstrate here that Markov state models (MSMs) can be used to study water dynamics in the complete continuum conformational space (spanned by positional and orientational angles and the relative separation) and to classify competing modes of H-bond rearrangements.

MSMs are useful to describe the slow dynamics in systems with many degrees of freedom, for example protein folding or protein ligand-binding [28–30]. Only few studies applied MSMs to solvent degrees of freedom[31, 32], mostly because the time scales are rather short so that the Markovian description might not be valid and since the diffusion processes make it difficult to define the proper subspace of relevant solvent degrees of freedom. We develop MSMs as a diagnostic tool to analyze and understand the complex multi-dimensional solvent dynamics. Based on simulation trajectories of liquid pure water at ambient temperature $T = 300$K, we construct a MSM in the twelve-dimensional configurational space of three water molecules and show that a number of slow processes in the ps range can be distinguished and analyzed in terms of the cooperative rearrangements of the H-bond pattern. We next analyze H-bond switching events de-

fined here as the process where a given central water molecule acts as a donor and the accepting H-bond partner switches from one water molecule to a different one. This H-bond switching event has been identified as the central element of H-bond dynamics in liquid water and consequently it has been amply studied. We perform a full MSM analysis of this H-bond switch scenario and provide the complete transition pathway network and analyze the competing transition probabilities.

II. METHODS

A. Markov state modeling

Markov state models describe complex dynamics of an arbitrary system by a Markovian stochastic process. Relevant degrees of freedom are projected onto a finite number of discrete states and the rates or transition probabilities between different states are described by a transition probability matrix $\mathbf{T}$. From this matrix transition times, transition paths and their probabilities can be extracted [33–35]. First, the state space has to be partitioned into N states. This is difficult for a diffusive system like water, since the state space depends on the set of water molecules that interact with each other, which obviously changes with time. From a simulated trajectory the $N \times N$ transition probability matrix $\mathbf{T}$ is calculated. The elements T_{ij} describe the conditional probability of a transition from state i to j within a fixed lag time τ and are estimated by $T_{ij}(\tau) = c_{ij}(\tau)/\sum_j c_{ij}(\tau)$, where $c_{ij}(\tau)$ is the number of transitions from state i to j within time τ and $\sum_j c_{ij}(\tau)$ is the number of transitions from i to any other state within time τ. The matrix is defined in such a way that the sum of every row is unity, thus, it conserves probability. We assume that the transition matrix is ergodic (any state can be reached from any other state within a finite number of steps), which yields a single eigenvector π with eigenvalue unity, the stationary distribution. For an MD simulation in equilibrium the detailed balance assumption $\pi_i T_{ij} = \pi_j T_{ji}$ holds. The N-dimensional vector $\mathbf{p}(t)$ describes the probability to be in one of the N states at time t, the probability at time $t + \tau$ follows from $\mathbf{p}(t + \tau) = \mathbf{p}(t)\mathbf{T}(\tau)$. The system is Markovian if it fulfills the Chapman-Kolmogorov equation

$$\mathbf{T}(n\tau) = \mathbf{T}^n(\tau). \tag{1}$$

A spectral decomposition of the transition matrix according to

$$\begin{aligned}\mathbf{p}(n\tau) &= \mathbf{p}(0)\mathbf{T}^n(\tau) \\ &= \sum_{i=1}^{N} \lambda_i^n \cdot (\mathbf{p}(0) \cdot \mathbf{r}_i) \cdot \mathbf{l}_i^T \\ &= \sum_{i=1}^{N} e^{-n\cdot\tau/t_i^*} \cdot (\mathbf{p}(0) \cdot \mathbf{r}_i) \cdot \mathbf{l}_i^T, \end{aligned} \tag{2}$$

where $\mathbf{r}_i$ and $\mathbf{l}_i^T$ are the $i-$th right and left eigenvectors of the transition matrix, yields characteristic time scales

$$t_i^* = -\frac{\tau}{\ln \lambda_i} \tag{3}$$

that are directly related to the eigenvalues of the eigenvector and should be independent of the lag time τ. Eq. (2) describes the evolution of the probability density distribution as a superposition of left eigenvectors that are weighted by their eigenvalues or time scales. In a nutshell, the construction of a Markov state model requires (i) clustering of the state space, (ii) estimating the transition matrix, and (iii) checking the validity of the Markov model by investigating if Eq. (1) is fulfilled, see SI text for details.

From the transition matrix transition pathways can be extracted that lead from the subspace of reactant states A to the subspace of product states B and pass through the subspace of intermediate states I. The solution of the linear system of equations

$$-q_i^B + \sum_{k\in I} T_{ik} q_k^B = -\sum_{k\in B} T_{ik} \tag{4}$$

defines the committor probability q_i^B, which describes the probability of reaching B before returning to A when being in state i. The flux along the intermediate states i and j which contribute to transitions from A to B is described by

$$f_{ij} = \pi_i q_i^A T_{ij} q_j^B, \tag{5}$$

from which the net-flux follows as $f_{ij}^B = \max\{0, f_{ij} - f_{ji}\}$. The reaction rate k_{AB} is given by

$$k_{AB} = \sum_{i\in A}^{N} f_{ij} \Big/ \left(\tau \sum_{i=1}^{N} \pi_i q_i^A\right). \tag{6}$$

The set of states and net fluxes creates a transition network, which can be decomposed into individual transition pathways with different probabilities, see SI text for details.

B. Molecular Dynamics Simulations

The MSM is based on a molecular dynamics (MD) simulation of 895 SPC/E water molecules in a cubic box of

edge length $L = 3$ nm with periodic boundary conditions. The trajectories are generated by GROMACS with a Berendsen weak coupling thermostat and barostat with a relaxation time of $t_{\rm rel} = 1$ ps for a fixed temperature of $T = 300$ K and a pressure of $p = 1$ bar. The time step of the MD simulation is 2 fs, every 20 fs the positional coordinates of every water molecule are stored and the total simulation time is 10 ns. The relative configuration of two water molecules is described by six coordinates: we fix a reference water molecule O* in the coordinate center with its two hydrogens in the $x-y$ plane such that the dipole vector points in the x direction, then we have three coordinates for the rotation (α, β, γ), see Fig. 1A, and three coordinates for the translation in spherical coordinates (R, ϕ, θ), see Fig. 1B. The rotation is described by Euler angles (α, β, γ) in the (z, x', z')-convention: A rotation around the z-axis by the angle α, a rotation around the new x-axis (x') by the angle β and a following rotation by the angle γ around the new z-axis (z'), see Fig. 1A. We also tested the use of quaternions for the description of the rotation, see SI text, which leads to equivalent results, but at the end used Euler angles. Consequently, for three water molecules the state space

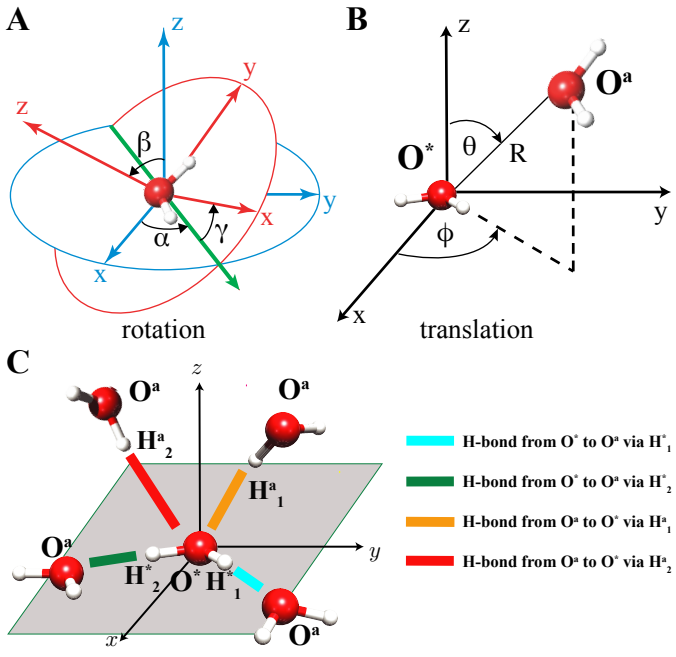

FIG. 1. **(A)** Euler angles are used for the rotational degrees of freedom and **(B)** spherical coordinates for the translational degrees of freedom. The reference water O* is placed in the coordinate center such that its two hydrogens are located in the $x-y$-plane and the dipole vector points along the x-axis. **(C)** Sketch of different H-bond configurations between two waters. In the cyan configuration O* acts as a donor via H_1^* to O^a, in the green configuration it donates via H_2^* to O^a. In the orange configuration O^a donates to O* via H_1^a, whereas in the red configuration it donates via H_2^a.

is 12-dimensional.

We base our definition of an H-bond on the distance-angle definition [36], where an H-bond exists if the distance between two oxygen atoms O* and O^a is $R < 0.35$ nm and the angle between the $\overline{O^*H^*}$ and $\overline{O^*O^a}$ vectors is $\angle(\overline{O^*O^a}, \overline{O^*H^*}) < 30°$. There are four ways in which two water molecules can establish an H-bond, see Fig. 1C for our color coding which we use throughout this paper. In the green and cyan configuration O^a accepts an H-bond from O*, whereas in the orange and red configuration O^a donates an H-bond to O* via H_1^a and H_2^a, respectively.

III. RESULTS AND DISCUSSION

A. H-bond rearrangements from three-water MSM

We base our MSM on trajectories for three waters, denoted by O*, O^a, and O^b, which are embedded in a liquid water environment. In order to select the suitable configurational subspace we determine the radial distribution function $g_{OO}(R)$ between two waters from which we calculate the free energy

$$F(R) = -k_{\rm B}T \ln\left[g_{OO}(R)\right] - k_{\rm B}T \ln(R^2), \qquad (7)$$

depicted in Fig. 2A and B. The yellow and green shaded domains correspond to the first and second hydration shells. A barrier of about $1k_{\rm B}T$ exists between the first and the second hydration shells.

In previous work we have determined the position-dependent diffusivity profile $D(R)$ between two water molecules using the so-called round-trip method, which maps the relative dynamics onto the generalized Fokker-Planck equation [37]. Our results in 2C show that for small separation distances $R < 0.3$ nm the diffusivity $D(R)$ is six times smaller than the bulk value. We compare these results with the diffusivity profile extracted from our MSM model, which is a nice consistency check of these two very different methods, see SItext for details.

The trajectories for the three-water MSM are selected as follows. We start recording the 12-dimensional trajectory as soon as the radial distance between O* and O^a, and between O* and O^b is < 0.5 nm. We stop recording when one of the two waters leaves the cutoff radius of 0.5 nm, see Fig. 3 for a sample trajectory. We captured 320,000 trajectories with a total length of 1700 ns and used the k-means++ algorithm [38] with 500 states to cluster states in the 12-dimensional state space. The transition probability matrix $\mathbf{T}(\tau)$ is estimated for a range of lag times and the time scales t_i^* are derived from the eigenvalues of each eigenvector according to Eq. (3). In Fig. 4A we plot the time scales against the lag time. The merging of time scales below 3 ps is caused by non-Markovian effects due to inertial effects. In the range from 3 to 20 ps the time scales are rather independent of the lag time and thus the dynamics is approximately Markovian. The small non-Markovian effects originate from a combination of projection errors and inertial effects, see [34] for an in-depth discussion. We observe

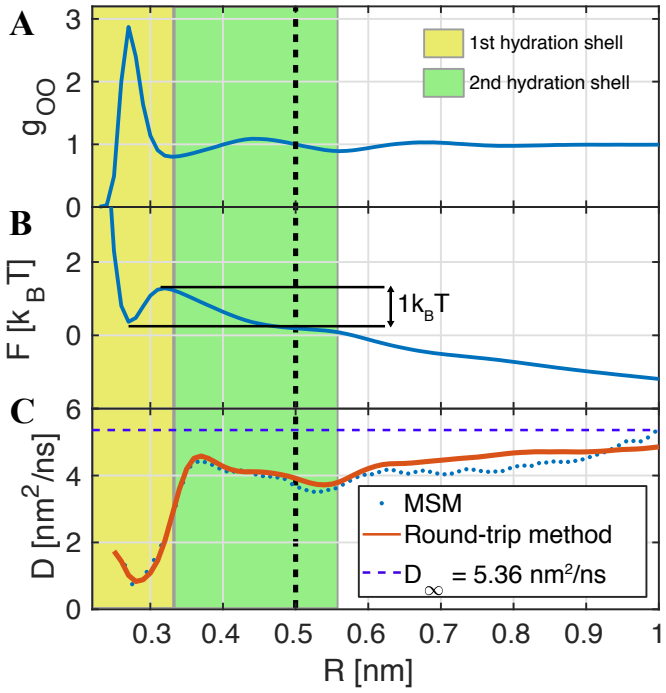

FIG. 2. **(A)** Radial distribution function $g_{OO}(R)$ between water molecules. $R = 0.5$ nm has been chosen as a cut-off for the selection of trajectories for the three-water MSM. **(B)** Free energy landscape $F(R)$. **(C)** Radial diffusivity profile $D(R)$ between two water molecules. The diffusivity profile calculated from the MSM is consistent with the profile estimated from the round-trip time method.

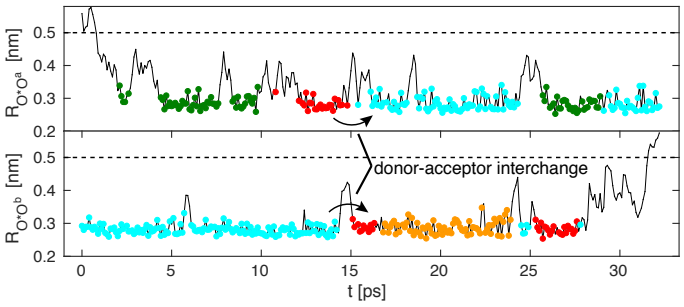

FIG. 3. Trajectories of the radial distances R between three waters. The different colors mark different H-bonds according to Fig. 1. Trajectories are used for constructing the MSM when both distances are smaller than 0.5 nm, denoted by broken horizontal lines. At $t = 15$ ps the O^a water molecules changes from a donor to an acceptor, whereas O^b changes from an acceptor to a donor.

that different time scales are fairly well separated from each other, which allows for a physical interpretation of the associated processes. For $\tau \geq 20$ ps the time scales merge again, which is due to limited sampling at large lag times, see SItext for a discussion. We choose the lag time $\tau = 7$ ps for the following analysis and project the 500 components of the eigenvectors onto the corresponding 500 clusters to understand the different processes. For

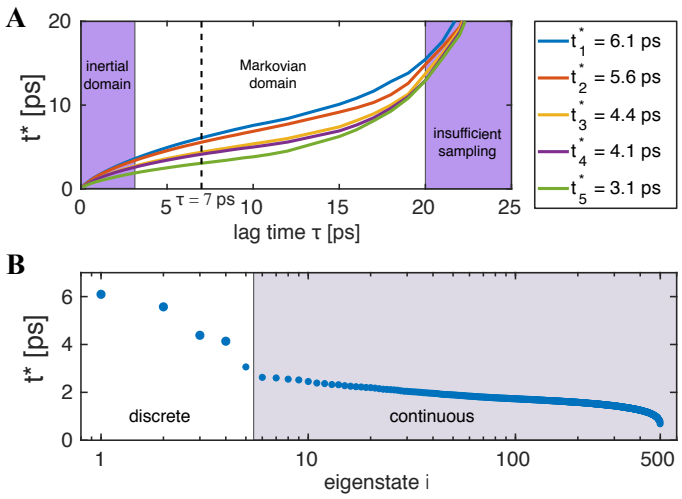

FIG. 4. **(A)** Plot of the five slowest time scales t_i^* versus the lag time τ. **(B)** Plot of all time scales for fixed lag time $\tau = 7$ ps. The five slowest time scales are separated from a continuum.

simplicity we only show the projection onto the angle ϕ for O^a and O^b.

The stationary distribution, depicted in Fig. 5A, indicates H-bonds between O* and O^a and between O* and O^b. The slowest process with a time scale $t_1^* = 6.1$ ps is depicted in Fig. 5B. The eigenvector contains negative components, which describe a loss of probability, and positive components, which describe the gain of probability. For O^a most of the green and cyan H-bond configurations (O* donates to O^a) are in the negative domain, whereas the red and orange H-bond configurations (O* accepts from O^a) are positive, see Fig. 5B. For O^b we observe the opposite, the red and orange configurations are negative and the green and cyan configurations are positive. This means that this eigenvector of the MSM can be interpreted as a transition where in the initial configuration O^a accepts an H-bond from O* and in the final configuration O^b accepts an H-bond from O*, as illustrated at the bottom of Fig. 5B. In other words, this process describes the interchange of donor and acceptor position of O^a and O^b, we therefore name it a donor-acceptor interchange. This process can be achieved by a concerted rotation of all three water molecules and it occurs in Fig. 3 at $t = 15$ ps, where water O^a changes from red to cyan (donating $\rightarrow$ accepting), whereas O^b changes from cyan to red (accepting $\rightarrow$ donating).

The second slowest process with a time scale of $t_2^* = 5.6$ ps, depicted in Fig. 5C, describes an acceptor-acceptor interchange. Here the cyan configuration of O^a describes the initial state whereas O^b is initially described by the green configuration. In the final configuration O^a and O^b have interchanged positions. Thus, we call this process an acceptor-acceptor interchange, which can be achieved by a rotation of the central water O* by 180° around its dipole axis.

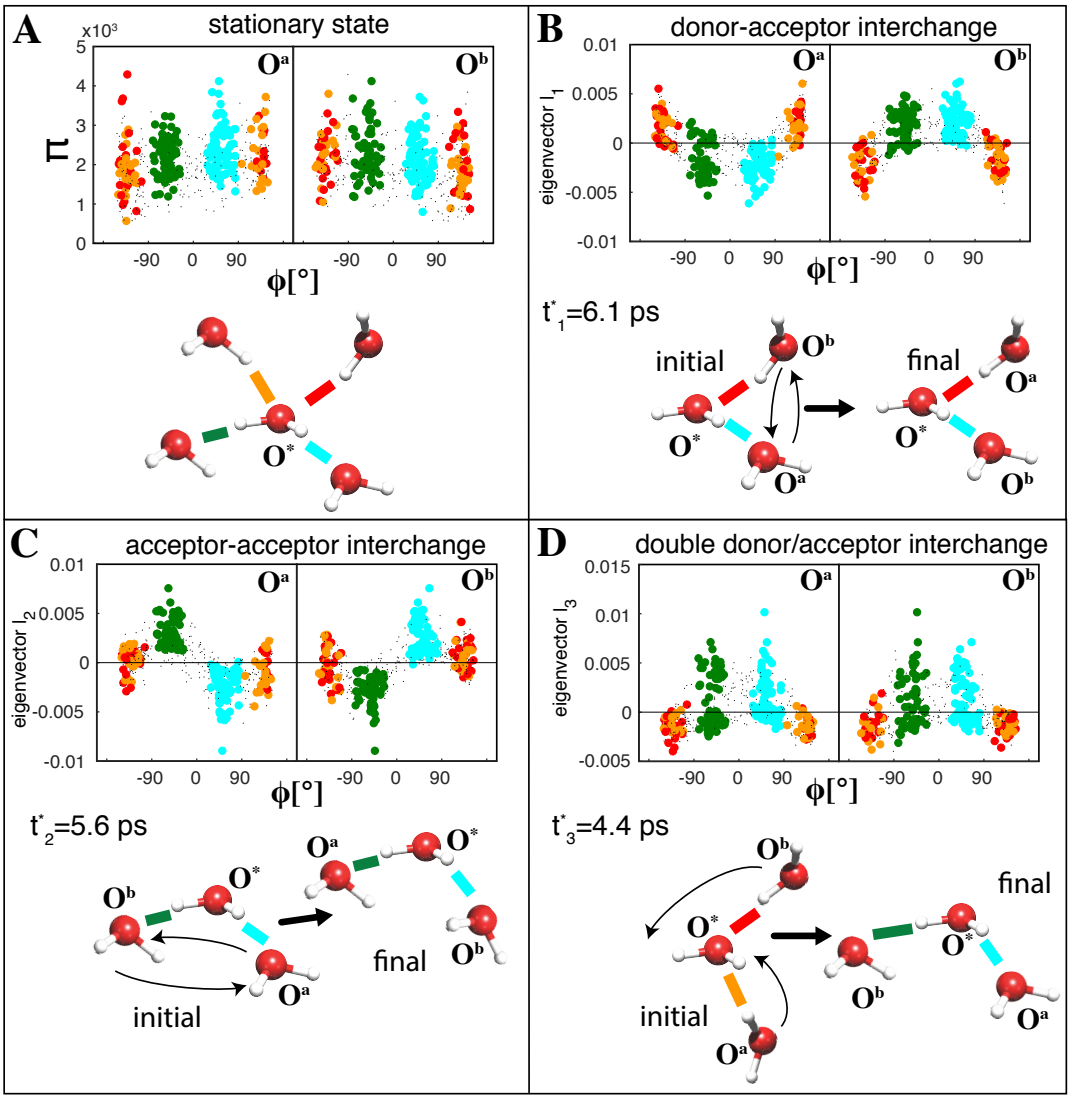

FIG. 5. **(A)** The equilibrium state consists of a combination of H-bonds between O* and waters O^a and O^b, the color coding for the type of H-bonds is described in Fig. 1. **(B)** The eigenvector with the slowest time scale $t_1^* = 6.1$ ps describes a donor-acceptor interchange, where O^a and O^b interchange their positions. This can be achieved by a rotation of all three waters O*, O^a, and O^b . **(C)** Acceptor-acceptor interchange. In the initial and in the final states O* provides H-bonds to both waters via its two H-atoms, in the final state O^a and O^b have interchanged positions. The time scale of this process is $t_2^* = 5.6$ ps. **(D)** Double donor/acceptor interchange. In the initial state O* accepts two H-bonds from O^a and O^b, whereas in the final state O^a and O^b accept H-bonds from O*. The time scale of this process is $t_3^* = 4.4$ ps.

We also discuss the third slowest process with $t_3^* = 4.4$ ps. Initially both waters (O^a and O^b) donate H-bonds to O*, whereas in the final state both waters accept H-bonds from O*, see Fig. 5D. This kind of transition corresponds to a concerted rotation of all three water molecules and we call it the double donor/acceptor interchange. The faster processes become more and more difficult to interprete.

We see that a three-water MSM nicely reveals the rearrangement of H-bonds in a water trimer. These cooperative rearrangements lead to considerably slower dynamics in the range of $4 - 6$ ps, compared to the typical librational time scale of $t_{\mathrm{libr}} \sim 200$ fs [16, 39, 40] or the reorientational time scale of $t_{\mathrm{reorient}} \sim 2.5$ ps it takes a water to change a single H-bond to another acceptor [10, 11, 14, 16, 41]. In fact, the presented processes involve the breaking of two H-bonds, a following concerted reconfiguration of the water trimer, and the subsequent formation of two new H-bonds. In [27] it was found from photon-echo experiments that a comparatively slow time scale in the 5 - 15 ps range exists that is related to H-bond rearrangements, our findings resonate well with this interpretation. It is remarkable that the four slowest processes we find within our MSM have rather similar time scales but describe very different structural rearrangements of the H-bonding pattern within the water

trimer. It would be very difficult to extract these dynamical modes from simulation trajectories without the MSM analysis. In SItext we show that a restricted MSM for a water dimer gives quite similar time scales but obviously does not allow to interpret the kinetic processes in terms of collective H-bond reconfigurations.

B. Transition paths for H-bond switching

In the previous section, we discussed kinetic processes that occur in a three-water MSM, but we have not analyzed the actual event when a hydrogen bond switches from one to another water molecule. The mechanism and the transition pathways of this switching event have been a challenging subject of research for decades [8]. In fact, this switching can be understood as a subset of the MSM discussed so far. In [7] it has been shown via transition path sampling that in roughly half of the cases when a H-bond is broken, a new H-bond forms right after. In [10, 11] it has been shown, that the mechanism is dominated by an abrupt angular rotation of the central water molecule. Here we will bring these two findings in harmony to each other and in particular will analyze the complete transition network that describes the switching of an H-bond.

In order to describe the switching event of a single H-bond by a MSM we modify the selection rule for trajectories. We now consider trajectories where O* is H-bonded to a water O^a via its hydrogen atom H_1^* initially and switches to a different water O^b to which it forms an H-bond via the same hydrogen H_1^*. We start recording trajectories when O* and O^a become H-bonded for the first time and stop when the H-bond between O* and O^b is broken finally, see Fig. 6A and B for two example trajectories.

We collect a total of 425,149 H-bond switching events and define four basis states which describe the H-bond configuration between two water molecules. In the bound state, called B, the central water molecule O* forms an H-bond with water molecule O^x by donating its hydrogen H_1^*, where the O^x stands for water O^a or O^b. In the unbound state, called U, there is no H-bond between O* and O^x and the radial distance between the waters is $R_{O*O^x} > 0.35$ nm, which exceeds the threshold separation for an H-bond. In the intermediate state, called I, there is no H-bond, but the distance between the two waters is $R_{O*O^x} < 0.35$ nm. In the alternative H-bond state, called H, the water molecule O* either accepts an H-bond from O^x or it forms an H-bond with O^x by donating its H_2^* to O^x, see Fig. 7A for an illustration of these four states. The combinations of these four basis states yields $4 \times 4 = 16$ MSM cluster states for three water molecules O*, O^a, and O^b. The validity of this restricted MSM for a lag time of $\tau = 3$ ps is checked in SI text.

In the reactant state O* and O^a are in state B whereas O* and O^b are in state U, which we denote as BU (i.e. the first letter denotes the type of H-bond between O* and O^a and the second letter denotes the type of H-bond between O* and O^b). The product state is defined as UB and is the opposite state as the reactant state BU, see Fig. 7B. We calculate the committor probabilities according to Eq. (4), the transition rate turns out to be $k_{\mathrm{BU}\to\mathrm{UB}} = 0.11$ ps^{-1} according to Eq. (6). This yields a reaction or mean first-passage time of

$$\langle t_{fpt} \rangle = 1/k_{\mathrm{BU}\to\mathrm{UB}} \approx 9.4\mathrm{ps}. \quad (8)$$

This time scale is similar to the time it takes two water molecules to diffuse from the first to the second hydration shell, which ranges between 4 to 12 ps depending on the target distance in the second hydration shell, see [37].

The 16 states and the net fluxes defined by Eq. (5) create a transition network, which can be decomposed into individual pathways that are characterized by transition probabilities, see SItext for the detailed derivation. We show the complete transition network in Fig. 7B. The thickness of the arrows indicates the net flux. States which contribute with a flux close to zero have been omitted, as a consequence of this the transition network in

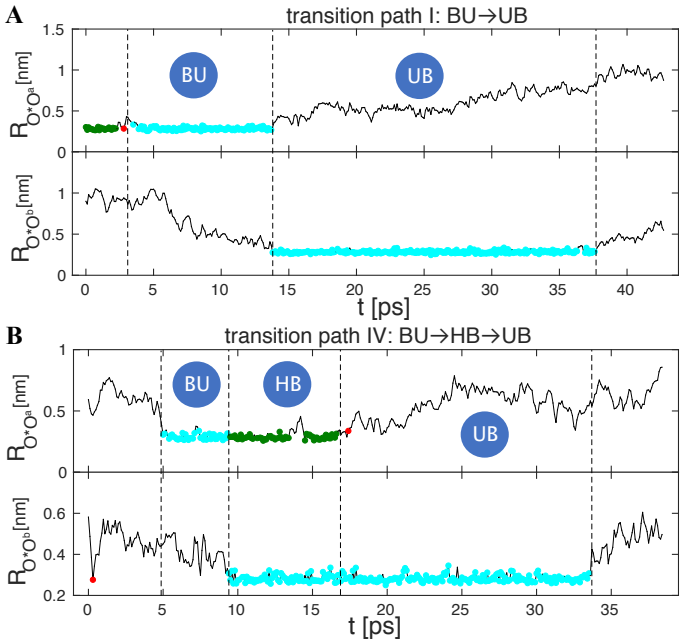

FIG. 6. Sample trajectories of H-bond switching events in terms of the radial distances between water molecules. (**A**) At $t = 4$ ps a H-bond (cyan color) between O* and O^a is formed for the first time. At $t = 14$ ps the H-bond of O* and O^a is broken and switches to O^b. O^a starts to diffuse away and O* and O^b stay H-bonded until the H-bond is finally broken at $t = 37$ ps. This process is an example for transition path type I, see Fig. 7C. **(B)**. At $t = 5$ ps an H-bond (cyan color) between O* and O^a is formed for the first time, is broken at $t = 9$ ps at which time it switches to O^b. In this trajectory, O^a does not diffuse away, but forms a different H-bond, where it accepts a hydrogen from O* (green color) until it diffuses away at $t = 16.5$ ps. This process is an example of a transition path of type IV, see Fig. 1 for color notation.

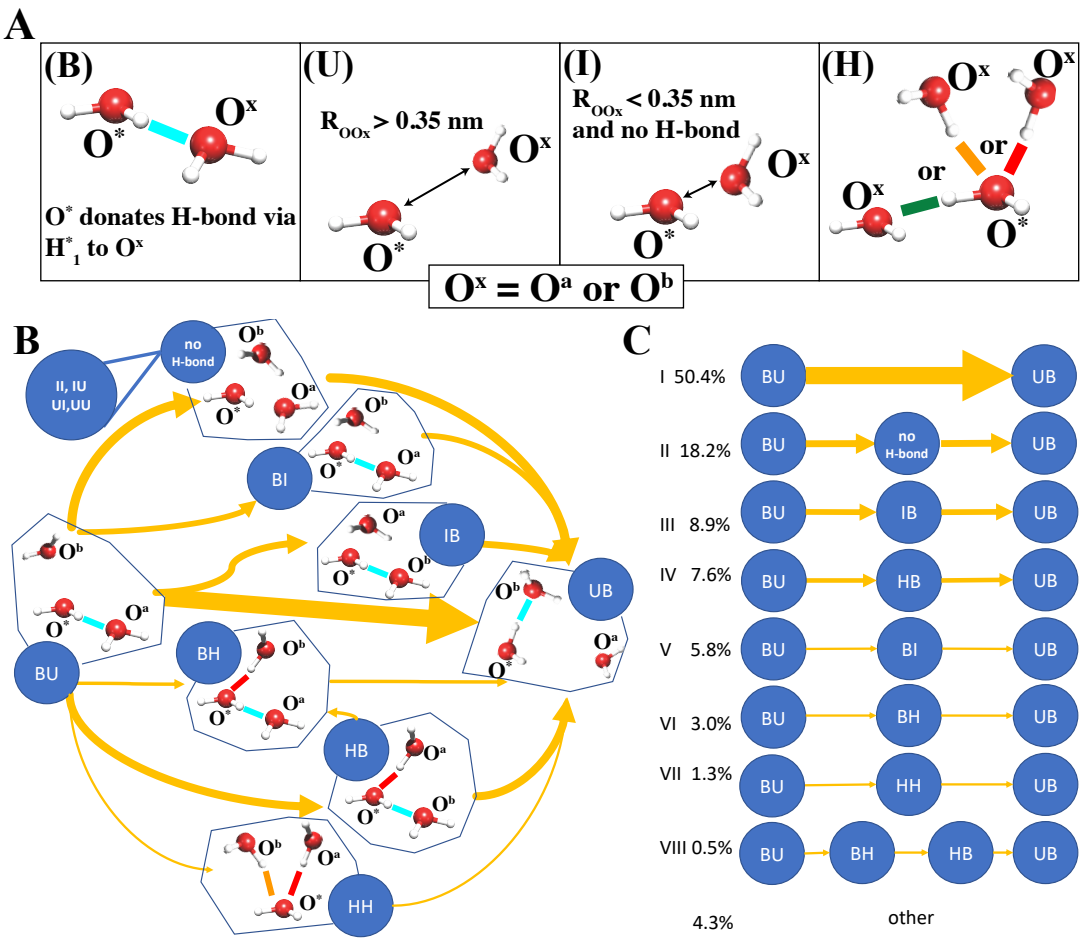

FIG. 7. **(A)** Basis states describing the H-bond between O* and another water molecule O^x. **(B)**Transition network for H-bond acceptor switching. States which are visited rarely are not shown, the arrows indicate the net-flux. In the reactant state BU, O* acts as a H-bond donor to O^a via H_1^*, while no H-bond with O^b is present and the distance between O* and O^b is larger than 0.35 nm. In the product state UB, O* acts as a H-bond donor to O^b via the same hydrogen H_1^*, while no H-bond with O^a is present and the distance between O* and O^a is larger than 0.35 nm. . **(C)** Transition paths ordered by their probabilities. Pathways with probability lower than 0.5% are not shown.

Fig. 7B shows only 11 of the 16 states. As the most important result, we find competitive pathways of H-bond switching. The main transition pathway (I) with a probability of 50.4% is the direct transition path BU→UB, where O* switches its donating hydrogen from O^a to O^b without an intermediate state (on the time scale set by the lag time of $\tau = 3$ ps), followed by an increase of the separation between O* and O^a above the threshold $R > 0.35$ nm. The third (III) and fifth (V) transition pathways involve the intermediate state I where a water (O^a or O^b) stays at a separation $R < 0.35$ nm before proceeding to the unbound state U. These three transition paths (I, III, and V) sum up to about two thirds of all possible transitions and involve no broken H-bond of O* as an intermediate. Thus, we find these transitions, which agree with the pathway described by Laage et al. [10, 11], to constitute the predominant set of pathways for H-bond switching, also in agreement with [7].

The next important pathway II consists of a short-lived intermediate state which can be of the II, IU, UI, or UU type, and has a probability of 18.2%. The last class of pathways, IV,VI,VII, and VIII, consists of intermediate states where O* forms an alternative H-bond with O^a or O^b, they sum up to a total probability of 12.4%. This class of four pathways deviates from the pathway described in [10, 11], for example, in pathway IV the O^a water does not immediately diffuse away from O*, but rather stays H-bonded to O* in a different configuration, see Fig. 6B.

IV. CONCLUSIONS

Using transition path analysis of Markov models we classify all possible pathways describing the H-bond switching from one acceptor to another acceptor. The dominating transitions ($\approx$ 66%) have been previously

identified [7, 10, 11] and correspond to a direct transition to the new H-bond acceptor without a broken H-bond as an intermediate state. A non-H-bonded intermediate in the transition pathway occurs only in about 18% of all transitions and the remaining fraction with a probability of 12% describes a different H-bond arrangement in the intermediate state. We conclude that the transition pathways we find for the single H-bond switch are consistent with previous findings but draw a finer and more complete picture of the H-bond reconfiguration dynamics that describes the switch from one H-bond accepting water to a different H-bond accepting water. In previous research [10, 11] the analysis did not resolve intermediate states, for example where the future H-bond accepting water molecule is already H-bonded to the central water molecule O* before becoming the accepting water molecule.

In the first part of the paper we identify the slowest dynamic processes occuring in a water trimer that is embedded in liquid water and relate them to concerted rearrangements of H-bond patterns. These processes consist of the concerted breaking and forming of two H-bonds, and correspond to donor-acceptor, acceptor-acceptor and double donor/acceptor interchanges. In previous quantum calculations the concerted breaking and forming of H-bonds in isolated water clusters has been characterized [21, 22, 42]. These studies suggest that H-bond rearrangments are local and do not involve more than three water molecules [21]. Nevertheless, it would be interesting to extend MSMs to tetramers or pentamers in order to check whether concerted H-bond rearrangements that involve more than three water molecules exist in the liquid state.

V. ACKNOWLEDGMENT

This work was funded by the Deutsche Forschungsgemeinschaft (DFG) by grant SFB 1114/C02.

[1] P. Ball, Chem. Rev. **108**, 74 (2008).
[2] Y. M. Rhee, E. J. Sorin, G. Jayachandran, E. Lindahl, and V. S. Pande, Proc. Natl. Acad. Sci. USA **101**, 6456 (2004).
[3] B. Kowalik, A. Schlaich, M. Kanduč, E. Schneck, and R. R. Netz, J. Phys. Chem. Lett. **8**, 2869 (2017).
[4] X. Huang, C. J. Margulis, and B. J. Berne, Proc. Natl. Acad. Sci. USA **100**, 11953 (2003).
[5] S. Sharma and P. G. Debenedetti, Proc. Natl. Acad. Sci. USA **109**, 4365 (2012).
[6] F. Sedlmeier, D. Horinek, and R. R. Netz, J. Am. Chem. Soc. **133**, 1391 (2011).
[7] F. S. Csajka and D. Chandler, J. Chem. Phys. **109**, 1125 (1998).
[8] F. H. Stillinger, Science **209**, 451 (1980).
[9] P. Debye, J. Soc. Chem. Ind. **48**, 1036 (1929).
[10] D. Laage, Science **311**, 832 (2006).
[11] D. Laage and J. T. Hynes, J. Phys. Chem. B **112**, 14230 (2008).
[12] D. Laage, G. Stirnemann, F. Sterpone, and J. T. Hynes, Acc. Chem. Res. **45**, 53 (2011).
[13] D. Laage, G. Stirnemann, F. Sterpone, R. Rey, and J. T. Hynes, Annu. Rev. Phys. Chem. **62**, 395 (2011).
[14] D. Laage, J. Phys. Chem. B **113**, 2684 (2009).
[15] K. Amann-Winkel, M.-C. Bellissent-Funel, L. E. Bove, T. Loerting, A. Nilsson, A. Paciaroni, D. Schlesinger, and L. Skinner, Chem. Rev. **116**, 7570 (2016).
[16] H. J. Bakker and J. L. Skinner, Chem. Rev. **110**, 1498 (2010).
[17] S. T. Roberts, K. Ramasesha, and A. Tokmakoff, Acc. Chem. Res. **42**, 1239 (2009).
[18] J. D. Eaves, J. J. Loparo, C. J. Fecko, S. T. Roberts, A. Tokmakoff, and P. L. Geissler, Proc. Natl. Acad. Sci. USA **102**, 13019 (2005).
[19] S. Habershon, T. E. Markland, and D. E. Manolopoulos, J. Chem. Phys. **131**, 024501 (2009).
[20] X.-Z. Li, B. Walker, and A. Michaelides, Proc. Natl. Acad. Sci. USA **108**, 6369 (2011).
[21] W. T. S. Cole and R. J. Saykally, J. Chem. Phys. **147**, 064301 (2017).
[22] J. O. Richardson, C. Pérez, S. Lobsiger, A. A. Reid, B. Temelso, G. C. Shields, Z. Kisiel, D. J. Wales, B. H. Pate, and S. C. Althorpe, Science **351**, 1310 (2016).
[23] C. J. Fecko, J. D. Eaves, J. J. Loparo, A. Tokmakoff, and P. L. Geissler, Science **301**, 1698 (2003).
[24] C. J. Fecko, J. J. Loparo, S. T. Roberts, and A. Tokmakoff, J. Chem. Phys. **122**, 054506 (2005).
[25] M. L. Cowan, B. D. Bruner, N. Huse, J. R. Dwyer, B. Chugh, E. T. J. Nibbering, T. Elsaesser, and R. J. D. Miller, Nature **434**, 199 (2005).
[26] L. D. Marco, M. Thämer, M. Reppert, and A. Tokmakoff, J. Chem. Phys. **141**, 034502 (2014).
[27] J. Stenger, D. Madsen, P. Hamm, E. T. J. Nibbering, and T. Elsaesser, J. Phys. Chem. A **106**, 2341 (2002).
[28] J. D. Chodera and F. Noé, Curr. Opin. Struc. Biol. **25**, 135 (2014).
[29] K. M. Thayer, B. Lakhani, and D. L. Beveridge, J. Phys. Chem. B **121**, 5509 (2017).
[30] F. Noé, C. Schütte, E. Vanden-Eijnden, L. Reich, and T. R. Weikl, Proc. Natl. Acad. Sci. USA **106**, 19011 (2009).
[31] P. Hamm, J. Chem. Phys. **145**, 134501 (2016).
[32] C. Gu, H.-W. Chang, L. Maibaum, V. S. Pande, G. E. Carlsson, and L. J. Guibas, BMC Bioinformatics **14**, S8 (2013).
[33] V. S. Pande, K. Beauchamp, and G. R. Bowman, Methods **52**, 99 (2010).
[34] J.-H. Prinz, H. Wu, M. Sarich, B. Keller, M. Senne, M. Held, J. D. Chodera, C. Schütte, and F. Noé, J Chem Phys **134**, 174105 (2011).
[35] G. R. Bowman, V. S. Pande, and F. Noé, Adv. Exp. Med. Biol. (2014), 10.1007/978-94-007-7606-7.
[36] R. Kumar, J. R. Schmidt, and J. L. Skinner, J. Chem. Phys. **126**, 204107 (2007).
[37] Y. von Hansen, F. Sedlmeier, M. Hinczewski, and R. R. Netz, Phys. Rev. E **84** (2011), 10.1103/physreve.84.051501.

[38] M. K. Scherer, B. Trendelkamp-Schroer, F. Paul, G. Perez-Hernandez, M. Hoffmann, N. Plattner, C. Wehmeyer, J.-H. Prinz, and F. Noé, J. Chem. Theory Comput. **11**, 5525 (2015).
[39] A. Luzar and D. Chandler, Nature **379**, 55 (1996).
[40] A. Luzar and D. Chandler, Phys. Rev. Lett. **76**, 928 (1996).
[41] Y. L. A. Rezus and H. J. Bakker, J. Chem. Phys. **123**, 114502 (2005).
[42] K. Liu, J. D. Cruzan, and R. J. Saykally, Science **271**, 929 (1996).